PCCP

Metal free earth abundant elemental red phosphorus: A new class of visible light photocatalyst and photoelectrode material

Journal:	*Physical Chemistry Chemical Physics*
Manuscript ID	CP-ART-11-2015-006796.R1
Article Type:	Paper
Date Submitted by the Author:	15-Dec-2015

Complete List of Authors:	Ansari, Sajid; Yeungnam University, Chemical Engineering Ansari, Mohammad; King Abdulaziz University, Center of Nanotechnology Cho, Moo Hwan; Yeungnam University, Chemical Engineering

Journal Name

ARTICLE

Metal free earth abundant elemental red phosphorus: A new class of visible light photocatalyst and photoelectrode material†

Received 00th January 20xx,
Accepted 00th January 20xx

DOI: 10.1039/x0xx00000x

www.rsc.org/

Sajid Ali Ansari,[a*] Mohammad Shahnawaze Ansari,[b] and Moo Hwan Cho[a*]

Developing high-performance photoctalyst and photoelectrode with enhanced visible light harvesting properties are essential for practical visible light photocatalytic applications. Noble metal-free, highly visible light-active, elemental red phosphorus (RP) was prepared by a facile mechanical ball milling method, which is a reproducible, low cost and controllable synthesis process. The synthesis used inexpensive and abundant raw materials because most RP hybrids are based on expensive noble-metal. The novel milled RP showed significantly enhanced photocatalytic and photoelectrochemical performance with a lower charge transfer resistance than commercial RP under wide visible photoirradiation, making it a feasible alternative for photocatalytic applications.

Introduction

Since the pioneering work by Fujishima and Honda on the catalytic splitting of water over a semiconductor under photoirradiation in 1972, the development of semiconductor-mediated photocatalysis has expanded significantly.[1-4] The effective use of solar light for the organic dye degradation and electrocatalytic water splitting for hydrogen production is an environmental friendly process and currently a hot topic for research as well as an effective solution for the worldwide energy crisis and environmental problems. On the other hand, the major drawbacks with semiconductors are their wide band gap, which limit the photocatalytic reaction under wide visible light irradiation. Therefore, to utilize wide visible-light absorption with ~43% of solar energy, the development of a photocatalytic system with a small band gap is an important and interesting objective for fulfilling the future energy demands.[1-4]

More recently, elemental semiconductors, such as selenium, α-sulfur and red phosphorous (RP), have been reported to be highly visible light responsive photocatalysts. Among these, RP is a promising earth abundant elemental photocatalyst for water splitting and the photodegradation of organic pollutants under visible light irradiation.[5-10] On the other hand, the photocatalytic efficiency of RP is limited because of the rapid recombination of photoinduced electron and holes under normal conditions. Several studies of RP-based hybrid photocatalysts generally used co-catalysts to improve the photocatalytic performance. For example, Wang et al.[6,7] fabricated Pt-loaded RP and a YPO_4 nanosheets/RP hybrid using a hydrothermal method and examined its photocatalytic activity. Yuan et al.[8] prepared RP/g-C_3N_4 heterojunctions with enhanced photocatalytic activity and Dang et al.[9] prepared $Ni(OH)_2$/RP composites by precipitation methods, which led to an enhancement in photocatalytic activity under visible light irradiation. Shen et al.[10] fabricated a black phosphorous-RP hybrid and further tested their photocatalytic activity. Nevertheless, most of these processes have been limited by the complicated procedures, harsh chemicals and high cost; hence, they cannot be considered to be environmental friendly processes. In addition, the co-catalyst, such as Pt, Ni, YPO_4, g-C_3N_4, and black phosphorous, used in the synthesis of red phosphorus-based hybrids are rare, expensive and leak toxic metallic ions during the reaction, which generally prevent their large scale application.

The fabrication of a co-catalyst free earth abundant elemental RP photocatalyst using a simple process can be an alternative way to utilize it for large scale application. To the best of the authors' knowledge, the preparation of noble-metal free and co-catalyst free, visible light active bare RP photocatalysts has not been reported.

In this study, a simple attempt was made to improve the photoresponse of commercial RP using a facile single step mechanical ball milling method, which is a reproducible, low cost and controllable synthesis process. The effects of the ball milling treatment time, *i.e.* 0h (RP-0h), 12h (RP-12h), 24h (RP-24h), 36h (RP-36h), and 48h (RP-48h), on the photoresponses of the RP were studied in terms of the light absorption, photocatalytic and photoelectrochemical behavior. Significantly enhanced photocatalytic performance and photoelectrochemical behavior were observed for the photodegradation of the model colored dye and non-colored organic compound, Rhodamine B (RhB) and 2-chlorophenol (2-CP), under visible photoirradiation compared to commercially obtained RP, which was attributed to the improved charge separation efficiency of the photoinduced electron holes in

[a] School of Chemical Engineering, Yeungnam University, Gyeongsan-si, Gyeongbuk 712-749, South Korea, Email: sajidansari@ynu.ac.kr, mhcho@ynu.ac.kr
[b] Centre of Nanotechnology, King Abdulaziz University, Jeddah 21589, Saudi Arabia

†Electronic Supplementary Information (ESI) available: [ln C/C_0 vs t plots, band gap energy plot, DRS, TEM, BET, XPS and XRD of RP]. See DOI: 10.1039/x0xx00000x

milled RP. Furthermore, the photoelectrochemical response, such as electrochemical impedance spectroscopy (EIS) and linear scan voltammetry (LSV), under dark and visible photoirradiation, also support the enhanced visible light-driven photocatalytic activities of RP.

Experimental

Materials methods

RP was purchased from Yakuri Pure Chemicals, Kyoto Japan and RhB & 2-CP were acquired from Sigma–Aldrich. Sodium sulfate (Na_2SO_4) was obtained from Duksan Pure Chemicals Co. Ltd. South Korea. Ethyl cellulose and α-terpineol were supplied by KANTO Chemical Co., Japan and fluorine-doped transparent conducting oxide glass (FTO; F-doped SnO_2 glass; 7 Ω/sq) was purchased from Pilkington, USA. All other chemicals used in this study were of analytical grade and used as received.

Methods

Phase characterization was accomplished by X-ray diffraction (XRD, PANalytical, X'pert PRO-MPD, Netherland) using Cu Kα radiation (λ = 0.15405 nm). The optical properties of the samples were analyzed by ultraviolet-visible-near infrared (UV-VIS-NIR, Cary 5000, VARIAN, USA) spectrophotometry equipped with a diffuse reflectance integrating sphere. The photoluminescence (PL, Kimon, 1 K, Japan) spectra of the samples were recorded over the scanning range, 200-800 nm, with an excitation wavelength of 325 nm. PL was conducted at the Korea Basic Science Institute, Gwangju Center, South Korea. The chemical state and surface composition was analyzed by X-ray photoelectron spectroscopy (XPS, ESCALAB 250 XPS System, Thermo Fisher Scientific U.K.) using monochromatized Al Kα x-rays (hν = 1486.6 eV). The size and size distribution of the RP particles were observed by field emission transmission electron microscopy (FE-TEM, Tecnai G2 F20, FEI, USA) at an accelerating voltage of 200 kV. The Brunauer–Emmett–Teller (BET) surface area was measured from the N_2 adsorption-desorption isotherms using an adsorption apparatus (ASAP 2020, Physisorption Analyzer Micromeritics Inc. USA). The photoelectrochemical and photocatalytic experiments were performed using a 400 W lamp with an intensity of 31 mW/cm^2 (λ > 500 nm, 3M, USA). EIS was performed using a three electrode cell with a 0.2 M Na_2SO_4 electrolyte using a potentiostat (VersaSTAT 3, Princeton Research, USA). The working electrodes were prepared in a similar manner to that in previous reports.[1-3] Briefly, 100 mg of RP was suspended in ethyl cellulose and α-terpineol, and resulting mixture was mixed thoroughly and then coated on a FTO glass electrode using the doctor-blade method. The RP-coated (FTO) glass was used as the working electrode. Ag/AgCl (3.0 M KCl) and a standard Pt sheet were used as the reference and counter electrodes, respectively.

Mechanical ball milling of commercial RP

Commercially available RP powder was milled in steel cells (250 mL) using hardened steel balls (diameter 15 mm, weight 32 gm) for times ranging from 0 to 48 h. Mechanical milling was performed in a horizontal oscillatory mill (Retsch, PM 400) operating at 25 Hz. The mixture ratio of steel balls and RP powders was approximately 15:1 by weight percent. The milled materials were used directly with no added milling media. The RP was milled for the selected time period, *i.e.* for 0 (RP-0h), 12 (RP-12h), 24 (RP-24h), 36 (RP-36h), and 48 h (RP-48h), at 250 rotations per minute. The milled RP was used for further studies.

Photodegradation test

The photodegradation of model organic pollutants in the presence of RP was evaluated by the degradation of an aqueous solution of RhB under visible photoirradiation. The photocatalytic experiment was carried out by taking 4 mg of each photocatalyst in five different 20 mL RhB (10 mg/L) and 20 mL 2-CP (10 mg/L) solutions. Before visible light irradiation, the suspensions were agitated magnetically for 30 min in the dark to achieve adsorption-desorption equilibrium. The suspensions were then irradiated with visible light and every 1 h, a 2 mL sample was taken and the catalyst was separated by centrifugation to obtain a clear liquid. The degradation rate of the RhB solution at given intervals of irradiation were analyzed using a UV–vis spectrophotometer. The degradation efficiency of the photocatalyst was determined using the method reported elsewhere.[1-3]

Visible light induced photoelectrochemical studies (EIS and LSV)

The visible light-induced photoelectrochemical performance of RP-0h and RP-36h were examined using EIS and LSV in the dark and under visible photoirradiation. The EIS and LSV experiments were conducted in 50 mL of an aqueous electrolyte of 0.2 M Na_2SO_4. To evaluate the separation efficiency of the photoinduced electrons and holes over the RP surface, EIS was performed in the dark and under visible photoirradiation at a 0.0 V and 10 mV potential and at frequencies ranging from 1 to 10^4 Hz. The photocurrent response was measured by LSV in the presence and absence of photoirradiation at a scan rate of 50 mV/s over a potential range, -0.9 to +0.9 V.

Results and discussion

Proposed schematic illustration of the mechanical milling of RP

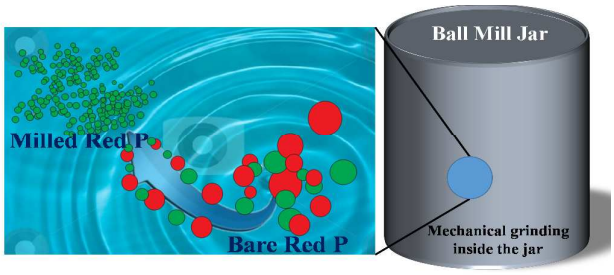

Fig. 1 Proposed schematic diagram of the mechanical grinding of RP in the ball mill,

Fig. 1 presents the working mechanism behind the improvement in crystallinity, reduction of the crystal size of RP through a high energy ball milling technique. The commercial bulk powder of RP was milled in several steps, *i.e.* for 12, 24, 36, and 48 hours. In the initial stages (0-12h), it was assumed that the micrometer sized material was crushed into irregular shapes. With further milling, they were converted to their nanosized dimensions.[11,12,13] During the reduction process, the RP particles are

under highly stressed conditions, which is due to impact with the high speed stainless steel balls and shearing between the grinding media and the cylindrical shell. As a result, the relevant compressive force normal to the RP particle surface and the ball leads to a miniaturization process with the evolution of shearing forces. The shearing forces weaken the van der Waals bonds between the molecules, which gradually decrease the micrometer particle size of the RP material to the nanometer range. The high crystallinity in this material is achieved by the conversion of primarily existing crystalline phases in the raw/initial material into the majority phase by ball milling. The process of crystallization in RP nanopowder can be understood by the decrease in dislocation density and the formation of nanograins with dislocation free lattices.[11,12,13]

Visible light photocatalytic performance

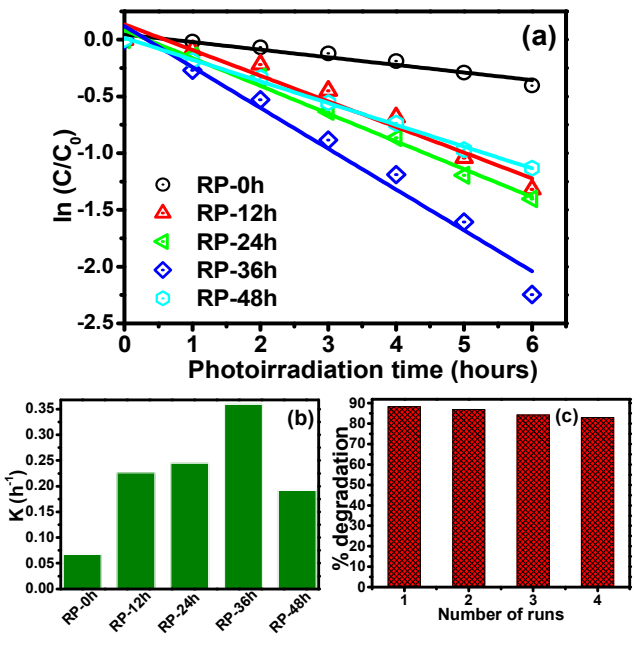

Fig. 2 (**a**) Logarithmic change in concentration (ln (C/C_0)) of RhB by RP-0h, RP-12, RP-24, RP-36, and RP-48h as a function of the visible photoirradiation time, (**b**) Rate constants for the photocatalytic degradation of RhB by RP-0h, RP-12, RP-24, RP-36, and RP-48h under visible photoirradiation, and (**c**) Cyclic stability of RP-36h towards the degradation of RhB under visible photoirradiation.

The influence in different milling time (RP-0h, RP-12h, RP-24h, RP-36h, and RP-48h) on the photocatalytic activity of RP under visible photoirradiation was examined. The model RhB organic pollutant degradation reaction was chosen, because this is stable fluorescence colored dye that is frequently used in the photochemical industries and textile industries. Fig. 2a shows a kinetic plot of the degradation RhB as a function of the irradiation time. The degradation of RhB as a function of the reaction time for the RP-0h and milled RP was fitted to pseudo-first-order kinetics according to the equation reported elsewhere.[4] A blank reaction with the catalyst in the dark (Fig. S1a) and without the catalyst in the light (Fig. S1b) confirmed that the self-degradation of RhB was negligible. Fig. 2b presents the rate constants (k) of the RP-0h and milled RP for the degradation of RhB. The corresponding k plot clearly indicated that the RP milled for 36h (RP-36h) exhibited much higher degradation rate, which is approximately 6 fold higher rate constant than that of commercial RP (RP-0h). The significant enhancement of the photocatalytic activity of the milled of RP was investigated by surface area analysis because mechanical grinding reduces the size of red P and increases its surface area.[11] In addition, a larger surface area of a photocatalyst is favorable for photocatalytic reactions because it is provides good contact between the dye and the photocatalyst.[11] The surface area of the RP-0h and RP-36h was 2.0613 m^2/g and 4.4176 m^2/g (Table S1), respectively. The surface area of the RP-36h was approximately 2.5 times higher than that of RP-0h, which is also accordance with TEM analysis. On the other hand, the RP milled for 48 (RP-48h) exhibited lower photocatalytic activity than RP-36h. This lower photocatalytic activity of RP-48h was attributed to the agglomeration of fine particles due to the increased milling time, which leads to a decrease in surface area (3.12 m^2/g) and photocatalytic activity. The high photocatalytic performance of the RP-36h was attributed mainly to the large surface area, improvement in the crystallinity, small crystal size and enhanced visible light absorption capacity due to the narrow band gap (Fig. S2).[5,14,15] In addition, photodegradation efficiency obtained in this case was also much higher than that our previously reported for modified metal oxides (TiO_2 and ZnO), suggesting the suitability of the RP-36h for environmental remediation processes.[1-4] In addition, the photocatalytic degradation ability of RP for the degradation of a non-colored phenolic compound, i.e. 2-CP, was also examined under similar experimental conditions to avoid the sensitization effect of the colored dye under visible light irradiation (Fig. S3). The k value for the visible light degradation of 2-CP by the RP-36h (0.1523/h) was ~5 times higher than that of RP-0h (0.0324/h). The results also suggest that the photocatalytic activity had been improved significantly by the mechanical grinding of RP.

The cyclic stability test of the RP-36h after the degradation of RhB was performed by centrifuging, washing and drying the catalyst. The reused RP-36h photocatalyst showed good recycling ability for up to four runs (Fig. 2c), which highlights its stability and reusability.

In comparison with other previously reported metal-based RP composites (Table 1), the milled RP (metal or supporting co-catalyst free) photoctalysts shows a substantial improvement in visible light photocatalytic activity.

Table 1: Comparison of photocatalytic performance of the prepared RP (current work) with the other previously reported RP based composite photoctalyst.

Photoctalyst based on RP	Co-catalyst and/or supporting catalyst	Improvement in the photocatalytic performance
Milled RP Current work	None	~6 times
RP/YPO_4	YPO_4	~6 times[7]
$RP/g\text{-}C_3N_3$	$g\text{-}C_3N_3$ and Pt	~10 times[8]
$RP/Ni(OH)_2$	$Ni(OH)_2$	~1.12 times[9]
RP/BP	BP	~2.87 times[10]
RP	Pt	~12 times[6]

Based on the above results, a possible photo excitation mechanism for the photocatalytic ability of the milled RP under visible photoirradiation is proposed, as shown in Fig. 3. Although the RP-0h have light absorption ability and simultaneous generation of photoinduced charge carriers, the photodegradation of RhB over RP-0h surface is negligible in comparison to RP-36. This is due to the amorphous behavior, low surface area and large number of photoinduced electron-hole trapping sites.

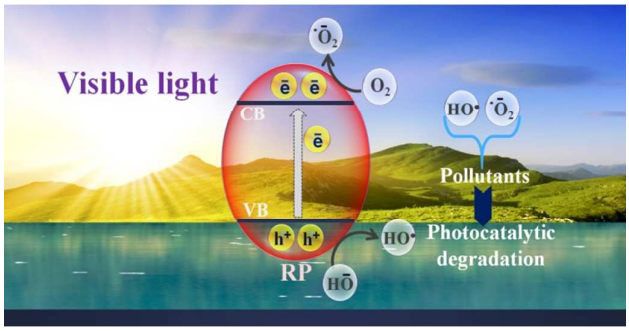

Fig. 3 Proposed photocatalytic mechanism for the photodegradation of RhB over RP under visible photoirradiation.

When milled RP is irradiated with visible light (Fig. 3), electrons are easily excited from the valence band to the conduction band due to a decrease in band gap energy (Fig. S2), leaving behind holes in the valence band. These photoelectrons can react with the surface-adsorbed O_2 to form superoxide radical anions.[5,6,8,11,16] The positive holes react with the surface-adsorbed hydroxyl ions to form highly reactive hydroxyl radicals. These radicals are mainly responsible for degrading the organic pollutants through a series of chemical reactions, as shown in Fig. 3. Generally, it is believed that the photocatalytic processes over the catalyst mainly depend on suitable photon energy absorption ability and effective separation of photoinduced charge carriers which are responsible for the production of highly active oxidation species. The improvement in the visible light absorption region alone cannot ensure high photocatalytic activity because the separation of the photogenerated electron-hole pairs and their migration to the surface reaction sites also plays an important role in determining the photocatalytic performance. The irradiation of visible light over RP-36h, the crystalline behavior might also promote visible-light absorption and the generation of photoexcited electron-hole pairs over the surface of RP-36h. The superior visible light photocatalytic activity of RP-36h can be explained based on the crystalline behavior and band gap narrowing. Shen et al.[14] in their crystalline phosphorus work, reported that crystalline behavior of RP greatly affects the optical properties and also favorable for the separation of photo-generated electrons and holes. The improvement in the crystalline behavior of RP-36h and band gap narrowing might have played a key role in increasing the photocatalytic activities of RP-36h. Following are the general reactions that occurred over the red phosphorous for the degradation of pollutants.

$RP + hv\ (visible\ light) \rightarrow e^- + h^+$

$e^- + O_2 \rightarrow O_2^{\bullet-}$

$h^+ + OH^- \rightarrow {}^{\bullet}OH$

$O_2^{\bullet-} + H_2O \rightarrow {}^{\bullet}OH$

${}^{\bullet}OH$ + organic pollutants (i.e. RhB) → pollutants degradation

Visible light-driven photoelectrochemical studies

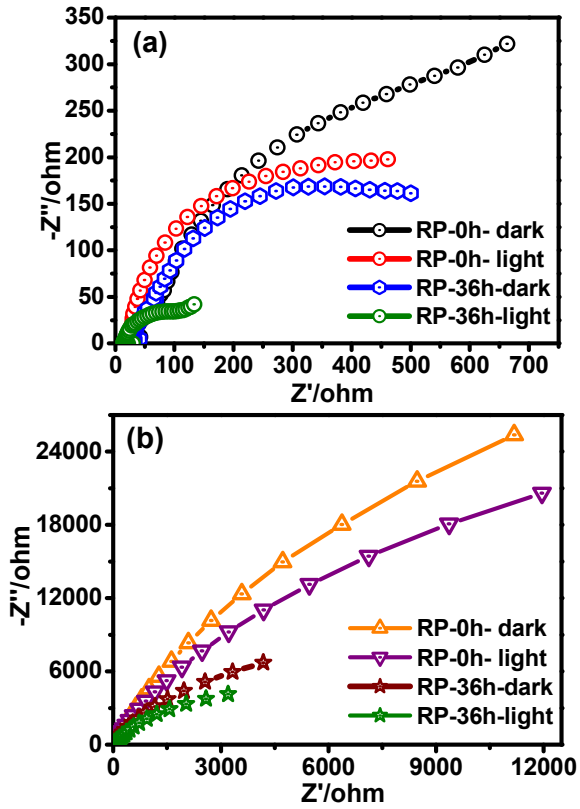

Fig. 4 EIS Nyquist plots at an applied potential (**a**) 0.0 V and (**b**) 10 mV of the RP-0h and RP-36h photoelectrodes in the dark and under visible photoirradiation.

The enhanced photocatalytic activity of milled RP was confirmed by EIS, which is helpful for examining the charge transfer resistance and separation efficiency between the photogenerated electrons and holes under visible photoirradiation.[2-4,11,12,17] The semicircular arc in the EIS spectra is an expression of the magnitude of charge transfer resistance at the photoelectrode/electrolyte interface. In other words, the smaller the arc radius, the smaller the charge transfer resistance and higher the efficiency of charge separation, which leads to a higher photoactivity of the materials. Fig. 4 presents the EIS Nyquist plot at an applied potential 0.0 V (Fig.4a) and 10 mV (Fig.4b) of the RP-0h and RP-36h in the dark and under visible photoirradiation. Fig. S4 presents the EIS Nyquist plot of RP-12h RP-24h in the dark and under visible photoirradiation. As shown in the figure, the arc radius of RP-36h was smaller than that of RP-0h (Fig. 4a and b), RP-12h (Fig. S4), and RP-24h (Fig. S4) under visible photoirradiation, which is because RP-36h has a lower resistance and effective separation of photogenerated electron hole pairs than RP-0h under visible photoirradiation. These obtained results under visible photoirradiation are in accordance with the photodegradation results of the RP-36h. Furthermore, EIS measurements of RP-0h and

RP-36 were also carried out in the dark and under visible photoirradiation at the open-circuit voltage to further correlate the improved photocatalytic performance of RP-36 (Fig. 4b). As shown in the figure, the illumination condition reduced the arc radius of RP-36 in the Nyquist plot. These results further indicate that a lower interfacial charge transfer resistance occurs between the as-prepared photoelectrode and electrolytes, which normally leads to greater effective separation of the photo generated charge carriers and faster interfacial charge transfer.[18]

In addition, to further confirm the enhanced photoactivity of RP-36h, LSV measurements were performed to measure the photocurrent response of RP-0h (Fig. 5a), RP-36h (Fig. 5a), RP-12h (Fig. 5b), and RP-24h (Fig. 5b) in the dark and under visible photoirradiation. Fig. 5a shows that RP-36h displays a better photocurrent response than the other RP photoctalysts. The significant enhancement in the photocurrent response of RP-36h was attributed to the increase in light absorption ability for the above-mentioned reason. The enhancement of photocurrent under visible photoirradiation further indicates fast transport of photogenerated electrons from RP to the current collector through the electrolyte. The EIS and LSV results are accordance with the photocatalytic activity of RP-36 under visible photoirradiation.

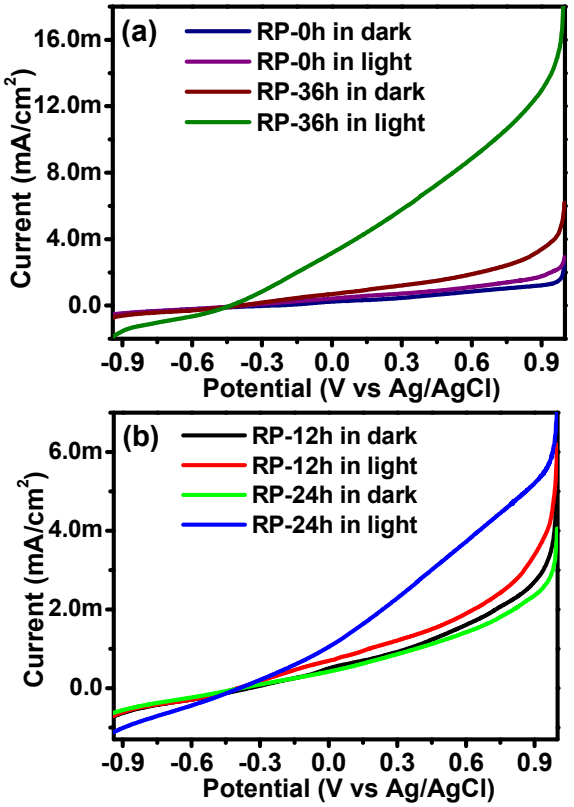

Fig. 5 Linear scan voltammograms of the (**a**) RP-0h & RP-36h, and (**b**) RP-12h & RP-24h photoelectrodes in the dark and under visible photoirradiation.

Structural and diffuse absorption studies

The structural properties of bare RP and milled RP (RP-12, RP-24, RP-36, and RP-48h) were examined by XRD. Fig. 6a shows the XRD pattern of the bare RP and milled RP. The XRD pattern of the milled RP and commercial RP showed peaks at ~15° and ~34.2° 2θ, which matched that reported in the literature and also confirmed the presence of only RP (i.e., no other form of phosphorous was present).[6-8,10,19,20] The XRD pattern of the RP milled at different times (0, 12, 24, 36, and 48h) showed no new peaks generated during the mechanical milling process, which also indicates the high purity of the sample. In addition, a thorough examination of the XRD patterns of the milled RP for different times revealed peak broadening, which also confirms the reduction of the crystal size of the milled RP according to the Scherer rule.[10] A similar XRD pattern of RP was also reported in the literature.[6-8,10,19,20] Furthermore, XRD of the RP-36h after degradation reaction revealed RP, which suggests that no structural deformity had occurred during photocatalytic degradation reaction (Fig. S5).

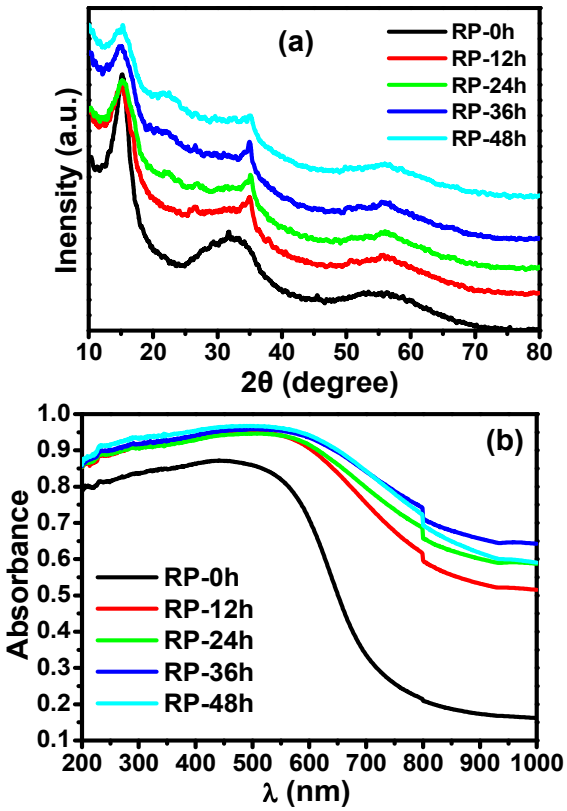

Fig. 6 (**a**) XRD pattern and (**b**) UV-visible diffuse absorbance spectra of unmilled (RP-0h) and milled RP for different times (RP-12, RP-24, RP-36, and RP-48h).

The light absorption properties of the commercial RP (RP-0h) and RP milled at different times (RP-12, RP-24, RP-36, and RP-48h) were analyzed by UV-visible diffuse absorbance/reflectance spectroscopy (Fig. 6b and S6). Both commercial and milled RP showed wide visible light absorption of the solar spectrum, which highlights the potential applications in visible light-driven photocatalysis. Interestingly, the milled RP exhibited a higher absorption edge in the visible region than the commercial RP (RP-0h). This shift in the absorbance edge of the milled RP in the visible

region is expected to improve the photocatalytic activity under visible light irradiation, and also suggests an improvement in its structure. In addition, the Kubelka-Munk functions versus the band gap energy plot were used to estimate the band gap of commercial RP and RP-36h (Fig. S2).[5-8,10,11,14,18] The estimated band gap of RP-0h was ~1.9 eV, which is similar to the previous reports, whereas RP ball-milled for the optimized time (RP-36) showed a band gap of ~1.45 eV. The band gap narrowing of RP-36 might be due delocalization of the molecular orbitals in the conduction band edge and the creation of shallow/deep traps in the electronic energy during the milling process, which resulted in a red shift of the absorption spectra.[21] In addition, the strain developed during the high energy ball milling process and small size of the RP-36h may also result in narrowing of band gap energy of the RP-36h.[21,22] This suggests that band gap reduction can modify the fundamental light absorption and photoinduced electron-hole formation during the photocatalytic reaction.[5-8,10,11,14,19]

Morphological studies

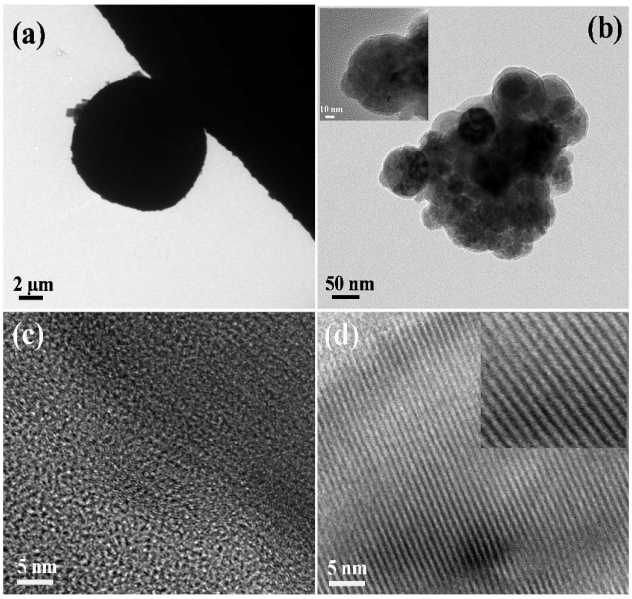

Fig. 7 TEM and HRTEM images of RP-0h (**a** and **c**) and RP-36 (**b** and **d**). The inset in figure **b** shows the size of RP-36h particle whereas inset of figure **d** shows the order or crystalline behaviour of RP-36h.

TEM and HRTEM were performed to further examine the morphology, size and obtain insight into the high photocatalytic activity of RP-36h. Fig. 7 and S7 shows the TEM image of the RP after 0h (Fig. 7a, S7a & b), 12h (Fig. S7c & d), 24h (Fig. S7e), 36h (Fig. 7b), and 48h (Fig. S7f) mechanical grinding. These images showed that the particle size of the commercially available bulk RP decreases with increasing milling time. On the other hand, the RP ground for 48h showed particle agglomeration (Fig. S7f). Fig. 7b & d, and S8 present the TEM and HRTEM images of RP-36. The TEM and HR-TEM images of the RP-36h clearly showed that size of the RP-36h had been reduced to the nm range compared to other RP photoctalyst after grinding, which would be helpful for increasing the surface area of red P-36h (Fig. 7b). The lattice images from the HRTEM image was clearly observed, which corresponds to the common crystalline allotrope of the Hittorf's phosphorous (Fig. 7d).[14,23] Compared to the HRTEM image of RP-0h (Fig. 7c), the HRTEM image of RP-36h (Fig. 7d) clearly showed more order or crystalline behavior, indicating that the structure is improved by mechanical grinding. The HRTEM was also performed at different places of the RP-36h sample, as shown in Fig. S8. Fig. S8 shows the lattice fringe spacing of the RP at different places. These results clearly show that mechanical grinding has significant effects on the crystallinity, size and surface area of the red P-36h, which is essential for high catalytic activity.

Raman spectroscopy is one of the most successful spectroscopic techniques used to examine the structural properties of materials. The Raman intensity of the material is generally associated with crystallinity of the samples. Therefore, it can be used to evaluate the degree of crystallinity of the materials. In general, crystalline materials present sharp and intense Raman peaks, whereas a less-ordered material will show less intense and wider Raman peaks.[24,25] Fig. 8 shows the Raman spectra of the RP-0h and RP-36h. The Raman peaks between 200-500 cm^{-1} were characteristic of red phosphorous, which is also consistent with the literature. As depicted in the figure, the milled RP showed more intense peaks than that of the unmilled RP. This could be because RP-36 has a more improved ordered structure than RP-0h. These results are also consistent with those reported by Li et al. in their study of crystalline red phosphorus-porous carbon nanofibers.[24,25]

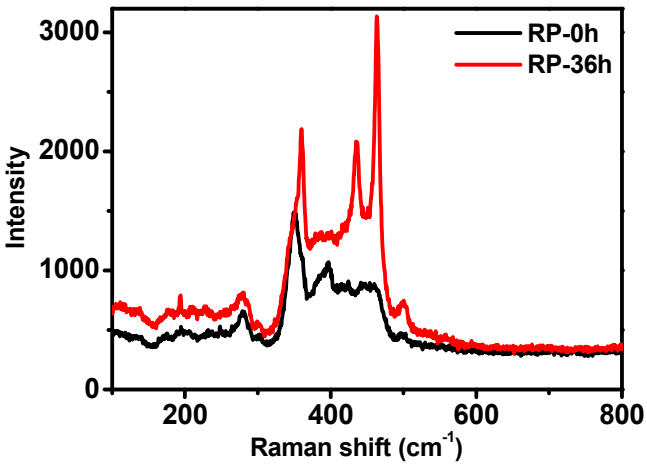

Fig. 8 Raman spectra of RP-0h and RP-36.

PL analysis

Photoluminescence spectroscopy is a widely used technique to examine the rate of recombination efficiency of photogenerated electron (e^-) - hole (h^+) pairs as well as the migration and transfer of charge carriers of various materials.[1-5] Fig. 9 shows the room-temperature PL spectra of the bare RP and milled red P. In general, a strong emission intensity means that the photoinduced e^- and h^+ are prone to recombination and the lifetime of the photoinduced e^- and h^+ is short, whereas a lower photoluminescence intensity means a

lower electron-hole recombination rate, and hence a longer lifetime of the photogenerated charge carriers. The RP-0h and RP-48h exhibits the strongest emission intensity, confirming the fastest charge recombination rate, whereas in the case of RP-36, the PL intensity was significantly reduced reduce after the mechanical grinding of RP, suggesting the slow photoinduced charge transfer in RP-36h. The PL spectra showed that an improvement in the crystalline behavior of the milled RP after ball milling could effectively inhibit electron-hole recombination during the photocatalytic reaction under visible photoirradiation. Sheni et al. reported that the improvement in the crystalline phase of red P can also greatly affect the optical properties, thereby influencing the absorption band edge and the change in PL intensity.[1-5]

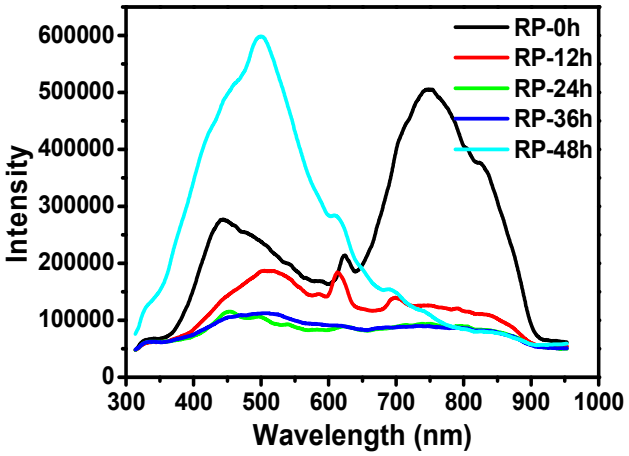

Fig. 9 PL spectra of RP-0h, RP-12, RP-24, RP-36, and RP-48h.

XPS analysis

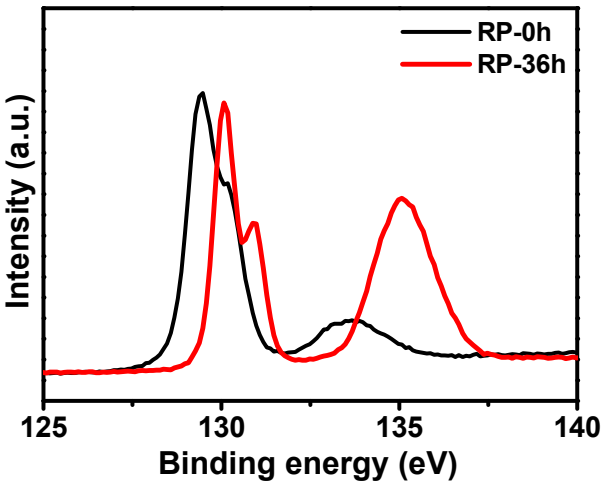

Fig. 10 P 2p core level XPS spectra of RP-0h and RP-36h.

Fig. 10 shows the P 2p core level XPS spectra of the pristine RP and milled RP. The P 2p peak was located at the binding energy (BE) of 129.45 ± 0.02 eV and 130.08 ± 0.02 eV for the pristine RP-0h and milled RP-36h, respectively.[7,10] The P 2p peak of the milled RP-36h shifted to a higher value compared to the pristine RP-0h. This larger shift of the BE was attributed to a change in crystallinity, which confirms the size reduction of the milled red P. A similar positive shift in the BE with decreasing particle size has been reported for a range of materials.[25] Overall, the positive shift of BE in the case of milled RP-36h was attributed to the decrease in the size and improvement in crystallinity.[26] The XPS binding energy analysis of RP-36h after degradation were examined and the results show that there were no significant changes in the BE of RP-36h after the degradation reaction (Fig. S9). This shows that the morphology and crystal structure of RP-36h are not affected significantly by the photodegradation reaction.

In addition to structural characterization, such as XRD, TEM, HRTEM, and XPS analysis, BET surface area measurements were also performed to evaluate the surface area of the bare RP-0h and milled RP. Table S1 shows that the RP-36h exhibit ~2.5 times higher surface area than RP-0h.

Conclusions

A visible light response was induced in RP using a mechanical ball milling method with a low-cost and earth abundant precursor of commercial RP for photocatalytic degradation and photoelectrochemical applications. The milled RP (RP-36h) exhibited remarkably enhanced photocatalytic activity and photoelectrochemical behavior compared to unmilled RP (RP-0h) under similar visible photoirradiation. These significantly enhanced performances obtained for RP-36h was attributed primarily to the smaller crystalline size, reduced band gap, improved crystallinity and enhanced surface area of the milled RP. In addition, the redshift in the absorption edge of milled RP and EIS charge separation analysis confirmed the enhanced charge separation play an important role in increasing the visible light activity of milled RP.

Acknowledgements

This study was supported by the Priority Research Centers Program through the National Research Foundation of Korea (NRF) funded by the Ministry of Education (2014R1A6A1031189) and by Basic Science Research Program (Grant No: 2015R1D1A3A03018029) through the National Research Foundation of Korea (NRF) funded by the Ministry of Education.

Notes and references

1 S. A. Ansari, M. M. Khan, S. Kalathil, A. Nisar, J. Lee and M. H. Cho, *Nanoscale*, 2013, **5**, 9238–9246.
2 M. M. Khan, S. A. Ansari, D. Pradhan, M. O. Ansari, D. H. Han, J. Lee, M. H. Cho, *J. Mater. Chem. A* 2014, **2**, 637–644.
3 S. A. Ansari, M. M. Khan, M. O. Ansari, M. H. Cho, *Sol. Energ. Mat. Sol. C.*, 2015, **141**, 162–170.
4 S. A. Ansari, M. M. Khan, M. O. Ansari, M. H. Cho, *New J. Chem.*, 2015, **39**, 4708-4715.
5 G. Liu, P. Niu, H. M. Cheng, *ChemPhysChem* 2013, **14**, 885–892.

6 F. Wang, W. K. H. Ng, J. C. Yu, H. Zhu, C. Li, L. Zhang, Z. Liu and Q. Li, *Appl. Catal., B*, 2012, **111–112**, 409−414.

7 F. Wang, C. Li, Y. Li and J. C. Yu, *Appl. Catal., B*, 2012, **119–120**, 267–272.

8 Y. P. Yuan, S. W. Cao, Y. S. Liao, L. S. Yin and C. Xue, *Appl. Catal., B*, 2013, **140–141**, 164-168.

9 H. Dang, X. Dong, Y. Dong, H. Fanb, Y. Qiu, *RSC Adv.*, 2014, **4**, 44823−44826.

10 Z. Shen, S. Sun, W. Wang, J. Liu, Z. Liu, and J. C. Yu, *J. Mater. Chem. A*, 2015, **3**, 3285–3288.

11 D. Chen, Z. Wang, T. Ren, H. Ding, W. Yao, R. Zong, and Y. Zhu, *J. Phys. Chem. C* 2014, **118**, 15300−15307.

12 J. Zhou, M. Zhang, Y. Zhu, *Phys. Chem. Chem. Phys.*, 2015, **17**, 3647−3652.

13 K. Zhu, W. Wang, A. Meng, M. Zhao, J. Wang, M. Zhao, D. Zhang, Y. Jia, C. Xu, Z. Li, *RSC Adv.*, 2015, **5**, 56239−56243.

14 Z. Shen, Z. F. Hu, W. Wang, Y. Li, S.-F. Lee, D. K. L. Chan, T. Gu, J. C. Yu, *Nanoscale*, 2014, **6**, 14163−14167.

15 M. C. Ortega-Liebana, J. L. Hueso, A. Larrea, V. Sebastian, J. Santamaria, *Chem. Commun.*, 2015, DOI: 10.1039/C5CC05387K.

16 W. Zhang, C. Kongab, G. Lu, *Chem. Commun.*, 2015, **51**, 10158−10161.

17 X. Ren, Q. Ma, H. Fan, L. Pang, Y. Zhang, Y. Yao, X. Rena and S. Liu, *Chem. Commun.*, 2015, DOI: 10.1039/C5CC06847A.

18 K. Kim, M.-J. Kim, S.-I. Kim and J.-H. Jang, Sci. Rep., 2013, 3, 3330 (1-8).

19 D. Xia, Z. Shen, G. Huang, W. Wang, J. C. Yu, P. K. Wong, *Environ. Sci. Technol.*, 2015, **49** (10), 6264–6273.

20 T.Yuan, Y. Heng, L. Feng, W. Yong-Long, Y. Shi-Hai, *J. Inorg. Mater.*, 2015, **30**, 653−661.

21 H. Lin, C. P. Huang, W. Li, C. Ni, S. I. Shah, Yao-H. Tseng, Applied Catalysis B: Environmental, 68, 2006, 1–11.

22 W.-J. Yin, S. Chen, J.-H. Yang, X.-G. Gong, Y. Yan and S.-H. Wei, Appl. Phys. Lett., 2010, 96, 221901 (1-3).

23 W. Hittorf, Ann. Phys. Chem. 1865, **126**, 193.

24 H. Hagemann, R. G. Snyder, A. J. Peacock, L. Mandelkern, Macromolecules, 1989, 22 (9), 3600–3606.

25 Willes H. Weber, Roberto Merlin, Raman Scattering in Materials Science, Springer Science & Business Media, Apr 18, 2013 - Science - 494 pages Springer: Berlin, 2000; Vol. 42.

26 I. Aruna, B. R. Mehta, L. K. Malhotra, S. M. Shivaprasad, *J. Appl. Phys.*, 2008, **104**, 064308.